ACS APPLIED MATERIALS & INTERFACES

Forum Article

www.acsami.org

Soft Nanocomposites—From Interface Control to Interphase Formation

Sascha A. Pihan,[†] Sebastian G. J. Emmerling,[†,§] Hans-Jürgen Butt,[†] Rüdiger Berger,*[,†] and Jochen S. Gutmann*[,†,‡,§]

[†]Max Planck Institute for Polymer Research, Ackermannweg 10, D-55128 Mainz, Germany

[‡]Johannes Gutenberg Universität Mainz, Saarstrasse 21, D-55128 Mainz, Germany

Supporting Information

ABSTRACT: We report measurements of structure, mechanical properties, glass transition temperature, and contact angle of a novel nanocomposite material consisting of swellable silsesquioxane nanoparticles with grafted poly(ethyl methacrylate) (PEMA) brushes and PEMA matrices with varying molecular weight. We measured the interparticle distance at the surface of the composites using scanning probe microscopy (SPM) and in the bulk of ∼0.5 μm thick films by grazing incidence small angle X-ray scattering (GISAXS). For a given molecular weight of the brush unstable dispersions at high molecular weight of the matrix indicate an intrinsic incompatibility between polymer-grafted-nanoparticles and homopolymer matrices. This incompatibility is affirmed by a high contact angle between the polymer-grafted-nanoparticles and the high molecular weight matrix as measured by SPM. For unstable dispersions, we measured a decreased glass transition temperature along with a decreased plateau modulus by dynamic mechanical thermal analysis (DMTA) which indicates the formation of a liquid-like layer at the brush−matrix interface. This proves the ability to decouple the structural and mechanical properties from the potential to be swollen with small molecules. It opens a new area of use of these soft nanocomposites as slow release materials with tailored mechanical properties.

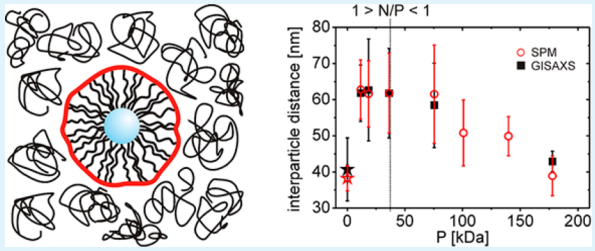

KEYWORDS: *nanocomposite, scanning force microscopy, GISAXS, polymer brushes, glass transition temperature, mechanical properties*

INTRODUCTION

By dispersing nanosized particles in polymer matrices one can add new functionalities, reduce the weight of fabricated components compared to conventional engineering materials like ceramics or steel, and furthermore enhance mechanical properties of polymeric materials.[1] The development of nanocomposites,[2] which consist of a polymer matrix and a nanoscale inorganic filler was therefore pushed forward within the last decades. In most cases, the filler is a spherical particle with a nonpenetrable surface. To enhance the compatibility of the inorganic fillers with the organic polymer matrix polymer brushes of the same chemical nature as the matrix are commonly attached onto the surface of the nanofillers.[3−5] A high compatibility is important for a homogeneous distribution of nanoparticles in the matrix. Many studies were carried out to identify the parameters that determine the miscibility of polymer-grafted-nanoparticles (polymer-*g*-nanoparticles) in polymer melts. A transition between dispersed and aggregated states was observed for a number of different systems, for example, PS-*g*-Silica,[6] PDMS-*g*-Silica,[7,8] or PMMA-*g*-Silica.[9] This transition can be explained theoretically by calculating the Gibbs energy *G* of a homopolymer chain with molecular weight *P* in contact with a brush of molecular weight *N*. It has been found that for a given grafting density the transition between stable and unstable dispersions is a function of N/P.[7,8]

In the field of material science, polymer-*g*-nanoparticles have been used to tailor polymers in terms of an increased storage and shear moduli[10] or glass transition temperature.[11,12] Many studies on such polymer-*g*-nanoparticles have focused on inorganic nanoparticles consisting of silicon oxide,[10,13] titanium oxide,[12,14,15,20] or metals.[5] In these studies, the nanofiller materials have a high elastic modulus compared to the modulus of the matrix polymer. It has been shown that the reinforcing effect of polymer-*g*-nanoparticles is controlled by the miscibility of the nanoparticles in the matrix[16] and the interparticle interactions such as diffusion and interpenetration of brushes and entanglement of grafted brushes with the matrix.[17] A few studies have focused on the influence of the properties of the core particles itself, especially for particles where the magnitude of elastic modulus is comparable to the modulus of the matrix.[18,19] The softness of the nanoparticles used in this study

Special Issue: Forum on Polymeric Nanostructures: Recent Advances toward Applications

Received: October 30, 2014
Accepted: March 9, 2015
Published: March 27, 2015

DOI: 10.1021/am507572q
ACS Appl. Mater. Interfaces 2015, 7, 12380−12386

may lead to applications where the particles act as containers for other molecules. These may then be released by external stimuli without a considerable change of the mechanical properties of the matrix. Typical container systems are hydrogels[21] used for drug delivery,[22] which can be stimulated by temperature,[23] pH,[24] or other stimuli.[25] An important property of these materials is their low Young's modulus which is typically in the range of a few hundred kPa to some MPa.[26−28]

When a solvent is evaporating from a mixture of polymers and impenetrable hard spheres, the polymer chains are getting more and more immobile during evaporation. The degree of the chain mobility has a strong effect on the local viscosity and thus influences the diffusion of nanoparticles within the matrix. For nanoparticles with a size bigger than the radius of gyration of the polymer chains, the diffusion of these nanoparticles is related to the macroviscosity of the polymer melt.[39] When the polymer melt reaches a glassy state by evaporation of solvent molecules, the nanoparticles are "frozen" at their position. However, the situation may change when the nanoparticles consist of a penetrable network which can also be swollen by solvent molecules. In this case, the diffusion of nanoparticles during evaporation of solvent molecules from the melt is influenced by the degree of swelling of the nanoparticles. In addition, the grafting of polymer brushes to such swellable nanoparticles influences the dispersion within polymer melts depending on the molecular weight ration of brush and matrix (N/P).

A common laboratory method to compound nanoparticles and matrix polymers is solvent blending. In this method, both, nanoparticles and matrix polymer are dispersed in a good solvent from which samples can be prepared either by spin coating, evaporation and molding or quenching in vacuum. Because of the presence of solvent molecules, the nanoparticles and the grafted brushes can swell to a significant degree. The swelling of the brushes allows the surrounding polymer to entangle with the brushes. The swelling of the nanoparticle may also allow molecules such as dyes, drugs or other functional molecules to diffuse inside the gel and being released upon external stimuli. When the solvent is evaporating from the composite we expect structural changes in the brush layer and between brushes and matrix during evaporation of the solvent. These structural changes of the interphase between matrix and brush layer may offer new possibilities to release drugs or tune mechanical properties of the composite. Moreover, depending on the N/P ratio, dispersed or agglomerated polymer-g-nanoparticles are expected. Furthermore, for composites applied as thin films, the dispersion of polymer-g-nanoparticles is determined by additional factors like the interaction with the free surface and the substrate as well as the brush-layer/matrix interactions.[29,30]

In a previous study, we have shown that the blending of soft polymer grafted nanoparticles improved the resistance of homopolymers against surface wear. Only at $(N/P) > 1$ the composites were reinforced, indicating entanglements between grafted brush and matrix polymer chains.[17] This improvement inspired us to study the mechanical properties and the nanoscale structure of thin films of such composites composed of soft nanoparticles and matrix polymer in more detail. Here we address the open question whether mechanical properties of a polymer-based composite containing swellable filler particles are determined by fact that the particles can be swollen or by the properties of the brush layer surrounding the cores. For this reason, we restrict this study to the case of athermal composites, i.e., a chemical identical brush and matrix polymer.. In this case, miscibility is determined by the grafting density of the brush layer, was well as the N/P ratio of brush to matrix molecular weight. Furthermore, since a swelling of the core invariably leads to a softening, we used PEMA as a more cohesive brush layer. Starting with PEMA poly n-alkyl methacrylates are known to form intermolecular bonds, which we expect to strengthen cohesion of the stabilizing polymeric shell.[44]

EXPERIMENTAL SECTION

The nanoparticles we used in our study are spherical nanoparticles consisting of amorphous products of organotrialkoxysilane condensations.[31] This family of silsesquioxane materials is constituted of silicon−organic network that can be swollen by solvent up to a swelling ratio of ∼4. The nanoparticles had a diameter of 18 ± 2 nm and a (R_g/R_h) ratio of 1.19 which indicates that the internal networks are loose and solvent can easily penetrate the particle interior. As the (R_g/R_h) ratio exceeds the theoretical value which is characteristic for hard spheres (0.775),[32] the particles can be considered as soft spheres. The grafting procedure of poly(ethyl methacrylate) brushes is based on the grafting of a silane terminated ATRP starter followed by a controlled radical polymerization as reported elsewhere.[33] The grafted brushes had a molecular weight (N) of 37.7 kDa as determined from GPC measurements of the brush polymer after dissolution of the silsesquioxane core.

The PEMA homopolymers which we used as matrix were prepared according to a receipt of Ramakrishnan et al.[34] We synthesized homopolymers with a variety of molecular weights (P) ranging from 11.7 to 269.2 kDa (Table 1).

Table 1. Properties of PEMA Homopolymers

abbr.	M_w [kDa]	PDI [M_w/M_n]
12k	11.7	1.20
19k	18.6	1.15
36k	36.4	1.12
75k	75.4	1.14
101k	100.9	1.21
140k	139.8	1.27
178k	177.8	1.28
269k	269.2	1.11

Film samples were from a solution of 10 mg of the PEMA-g-particles and 40 mg of PEMA homopolymer with 0.5 mL of toluene. The solid content in this mixture corresponds to a mass weight fraction of 20 wt % and a core volume fraction of 0.26. The solution was ultrasonicated for 30 min. Directly afterward, films were prepared by spin coating on silicon wafers (3000 rpm for 60 s) cleaned in an Ar-plasma (PDC-002, Harrick Plasma, USA). For reference we prepared dispersions of unmodified nanoparticles (without polymer brushes) and homopolymer in the same way. The thickness of the films was found to be between 400 and 500 nm as measured by a surface profiler (P-10, KLA Tencor, USA).

The surface topography of samples was analyszed by scanning probe microscopy (SPM) operated in tapping mode (Dimension 3100, Bruker, USA). Silicon cantilevers (OMCL-AC 160 TS, Olympus, Japan) with a nominal tip radius of ∼10 nm and a tip height of 11 μm were used.

The GISAXS experiments were done at the BW4 beamline of the HASYLAB @ DESY using the μ-focus option. We operated the experiments at a sample to detector distance of 2.0 m, a wavelength of λ = 0.138 nm and a beam size of 32 × 17 μm[35,36] (horizontal x vertical). For our experiments an incident beam angle of $\alpha_i = 0.7°$ was chosen. We performed transverse detector scans of the full 2D scattering pattern in reciprocal scattering plane ($q_{||}$) to extract the

DOI: 10.1021/am507572q
ACS Appl. Mater. Interfaces 2015, 7, 12380−12386

scattering curves. The transverse cuts were carried out at the maximum intensity of the Yoneda peak (α_c = 0.19°).[37] We deduced the correlation length of our samples from the position of the correlation peak in the scattering curves.

The DMTA measurements were performed using the Advanced Rheometric Expansion System (ARES, TA Instruments, Delaware, USA) in a parallel plate geometry. The studied materials were compress-molded as circular plates of 6 mm diameter and 1 mm thickness. Before the measurements, isothermal strain sweeps at different temperatures were performed to separate the linear from the nonlinear viscoelastic regimes. The shear deformation was applied with controlled deformation amplitude, which was kept in the range of the linear viscoelastic response of the studied materials. Frequency dependencies of the storage and the loss parts of the shear modulus have been determined from frequency sweeps measured within the frequency range 10^{-2}–10^{2} rad/s at various temperatures. Master curves for G' and G'' at a reference temperature have been obtained using the time–temperature superposition, i.e., shifting the data recorded at various temperatures only along the frequency coordinate. From the measured G'' the glass transition temperature was deduced at the maximum of the G'' versus temperature curve[38] as $T_g(G''_{max})$.

RESULTS AND DISCUSSION

To examine the swelling effect of the polymer-*g*-nanoparticles and the effect of the grafted polymer brushes on the dispersion in a polymer melt we imaged the surface of composites with different compositions using SPM. By analyzing the phase-contrast images of samples with a particle volume fraction Φ_c = 0.26, the polymer-*g*-nanoparticles appeared as bright spots and the homopolymer matrix as darker areas (Figure 1). In the case

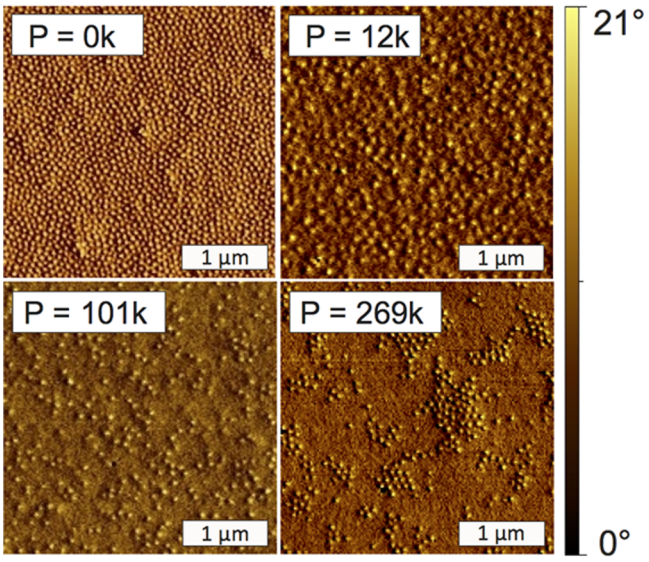

Figure 1. Phase-contrast images of PEMA-grafted μgels (Φ_c = 0.26) dispersed PEMA matrix homopolymer with different molecular weights. PEMA-grafted μgels appear as bright dots embedded in a matrix with darker contrast.

without a matrix homopolymer (Figure 1, P = 0k), we observed a dense packing of the polymer-*g*-nanoparticles. For the matrix with the lowest molecular weight we observed distributed polymer-*g*-nanoparticles (Figure 1, P = 12k). The dispersion became unstable (Figure 1, P = 101k) with a higher matrix molecular weight and finally aggregates (Figure 1, P = 269k) were formed.

To compare the different compositions more quantitatively, we analyzed the nearest neighbor distances $NN_{i,j}$ by using eq 1.

$$NN_{i,j} = \sqrt{(x_j - x_i)^2 + (y_j - y_i)^2} \quad (1)$$

Here, x_j, y_j are the coordinates of the particle of interest and x_i, y_i are the coordinates of every other particle in the image, respectively. $NN_{i,j}$ stands for all distances of particles among themselves ($0 < i, j < n + 1$). Here, n is the number of all particles observed. To determine the nearest neighbors NN_ν, we then took the minimum value of $NN_{i,j}$ distance for each particle "i". From the SPM measurements we deduced nearest neighbor interparticle distances ranging from 63 ± 8 nm for P = 11 kg/mol to 39 ± 6 nm for P = 178 kg/mol (Figure 2, unfilled

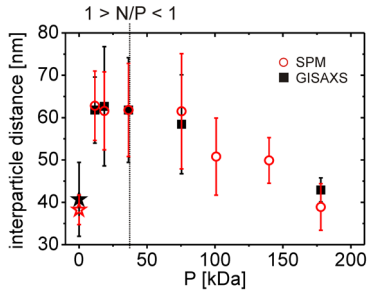

Figure 2. Nearest neighbor interparticle distance as a function of the molecular weight of the matrix polymer. Results from SPM (unfilled circles and GISAXS (filled squares) for a particle volume fraction of ϕ_c = 0.26. The dashed line indicates a N/P value of 1. The error bar in the SPM measurements is deduced from different samples and different measurement areas.

circles). In the sample where no matrix was present (P = 0) the interparticle distance was 38 ± 4 nm (Figure 2, unfilled star). Considering a core diameter of 18 ± 2 nm this yields a surface-to-surface interparticle separation, $ID_{s\text{-}s}$ of 20 ± 2 nm. For the pure cores the surface-to-surface interparticle separation $ID_{s\text{-}s}$ at a volume fraction of 0.26 would be 6.3 nm (based on the discussion by J.S. Meth et al. using ϕ_{max} = 0.637).[43] Additionally we carried out GISAXS measurements on the same samples to check whether the interparticle distance at the surface is different from the one in the bulk, since GISAXS measurements are uniquely able to probe both surface and bulk structures present in our samples. The GISAXS measurements on the same samples resulted in an interparticle distance of 62 ± 8 nm for P = 11k and 43 ± 3 nm for P = 178k (Figure 2, filled squares). In the sample where no matrix was present (P = 0) the interparticle distance was measured as 41 ± 9 nm (Figure 2, filled star). Thus we conclude that the interparticle distance at the surface does not differ from the interparticle distance in the bulk within the experimental error. This agreement shows that SPM images of the surface are representative for dispersion characteristics in the bulk material and the dispersion does not depend on the thickness of our sample. While in principle the surface energy of a free brush surface may differ from the interfacial energy of a brush matrix interface, we conclude that this difference does not play a major role in our system. This is a direct proof that the free energy of the contact to the matrix dominates. Even for surface bound particles as both PEMA and air are hydrophobic surroundings the perturbation by the free air interface is too small to result in a structural change to the particle layer at the surface.

Moreover, we also observed a transition from stable to unstable dispersions when the N/P ratio exceeds a value of 1 (Figure 2, dashed line) for our soft particles this implies that

DOI: 10.1021/am507572q
ACS Appl. Mater. Interfaces 2015, 7, 12380–12386

their dispersion behavior is similar to hard spheres. For N/P values smaller than 1 (left part of the graph), the dispersion is stable with a interparticle distances significantly larger than the interparticle separation $ID_{s\text{-}s}$ of 6.3 nm. For N/P values much larger than 2 (right part of the graph), the dispersion becomes unstable due to the wet−dry transition of the polymer brush. Theoretically such a phase transition is expected for N/P values ranging from approximately 1 (brushes on flat substrate) to 5 (brushes on a heavily curved core). The resulting phase separation of particles from the matrix leads to the formation of aggregates with a smaller interparticle distance that approaches the minimal the interparticle separation distance $ID_{s\text{-}s}$ observed in the pure particles samples (no matrix homopolymer present, denoted as P = 0 kDa). Since the core diameter is about twice the brush height and intermolecular attraction in PEMA the polymer chains,[44] it is sensible to conclude that the PEMA brushes on our particles do not show an increase in conformational freedom for the free brush ends. Therefore, the phase behavior tends toward the autophobic dewetting case for brushes on a flat substrate.

Experimental studies based on glass transition temperature measurements[40] suggest a surface-layer model to explain the thermomechanical behavior of thin polymer layers. In a further study the existence of a liquid-like layer at glassy surfaces was suggested by measuring the change in T_g of polymer films in contact with a hard surface of gold nanoparticles.[41] From our interparticle-distance measurements we hypothesize similar conditions for the polymer-*g*-nanoparticles in contact with polymer matrices. In the first case of a high M_w matrix polymer, the matrix does not wet the brush-layer (dry brush) and we consider the brush-layer as impenetrable for the long matrix chains. This consideration is affirmed by our nanowear tests on such composites (ref 17), where polymer-*g*-nanoparticles were torn out easily from high M_w matrices compared to particles in low M_w matrices. We assume the formation of a liquid-like layer at the interface between the dry polymer brush and the matrix polymer (Figure 3). The effect of this liquid-like layer should result in a decrease of the glass transition temperature and elastic modulus. In the second case of a low M_w matrix polymer, the brush-layer is swollen by the short matrix chains. In this case, we expect a gradual interphase, rather than a sharp interface, that does not influence the glass transition and the elastic modulus significantly.

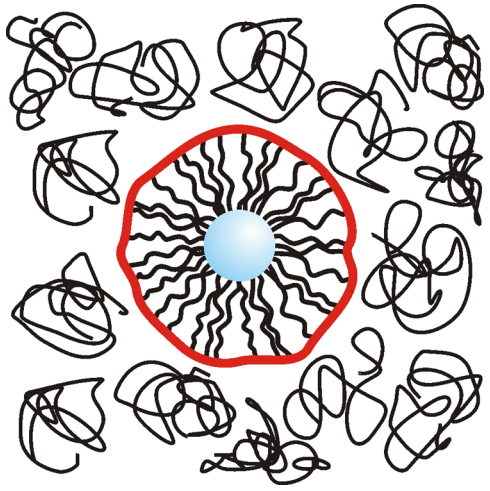

Figure 3. Sketch of a polymer-*g*-nanoparticle immersed in high M_w matrix polymer. If the brush layer on the core is in the dry brush regime (high matrix M_w), the whole particles acts as a hard sphere and a liquid-like layer (at the position of the red line) is is expected to be formed at the interface between brush-layer and matrix polymer.

This hypothesis of how these structures of dispersed and agglomerated nanoparticles influence the mechanical properties of the composite can be answered by dynamic mechanical thermal analysis (DMTA). The DMTA measurements enabled us to determine the glass transition temperature and the elastic modulus of the investigated composites simultaneously. Three composites with different molecular weight of the matrix where investigated. A low M_w matrix representing the well-dispersed state (P = 19k), a high M_w matrix representing the agglomerated state (P = 178k) and a matrix with intermediate M_w representing the phase transition between stable and unstable dispersions (P = 36 k). For all three molecular weights we prepared samples with a particle volume fraction ϕ_c of 0.26 and 0.49.

For samples where the polymer-*g*-nanoparticles were blended with homopolymer of M_w = 18.5 kDa we measured a plateau modulus of 440 kPa for the homopolymer and 520× and 480 kPa for the blended samples (Figure 4). Respective master-

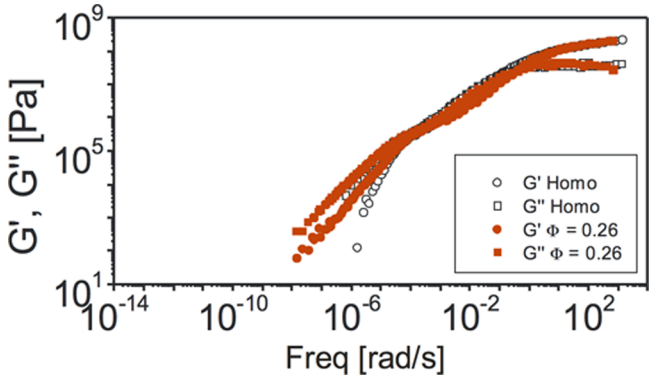

Figure 4. Mastercurves for blends of polymer-*g*-nanoparticles with homopolymers of M_w = 18.5 kDa for core volume fractions of 0.26 (filled symbols). The mastercurve of the neat homopolymer is represented by empty symbols.

curves for a volume fraction of 0.49 are given in the Supporting Information. No horizontal shift was observed for both composites compared to the homopolymer. The mastercurves show the same shape, implying similar mechanical behavior of the homopolymer and the composite. In both samples (ϕ_c = 0.26 and 0.49), we observed that they start to creep at higher temperatures (i.e., lower frequencies) than the homopolymer. The enhanced creep behavior might be regarded as a hint of improved interfacial interaction between polymer-*g*-nanoparticles and the homopolymer[42] and the formation of a interphase between them.

The results of DMTA measurements for a homopolymer matrix with M_w = 36.4 kDa and a blend of the same homopolymer and polymer-*g*-nanoparticles are shown in Figure 5. We measured a plateau modulus of 380 kPa for the homopolymer and for the composites 290 kPa (ϕ_c = 0.26) and 430 kPa (ϕ_c = 0.49), respectively. When the core volume fraction is increased to ϕ_c = 0.49 we observe a contribution of the nanoparticles to the plateau modulus of the composite as plateau modulus increases. Furthermore, for the composite with high volume fraction, the storage and loss moduli decrease faster than the moduli of the homopolymer in the frequency

DOI: 10.1021/am507572q
ACS Appl. Mater. Interfaces 2015, 7, 12380−12386

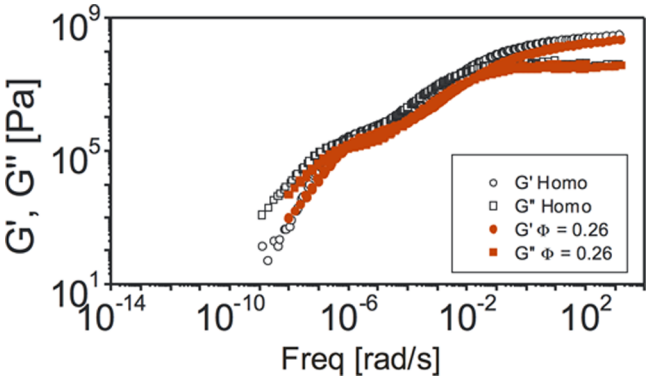

Figure 5. Mastercurves for blends of polymer-*g*-nanoparticles with homopolymers of M_w = 36.4 kDa for core volume fractions of 0.26 (filled symbols). The mastercurve of the neat homopolymer is represented by empty symbols.

regions corresponding to segmental flow and the rubbery response. This fast decrease shows that the polymer-*g*-nanoparticles have an effect on the elastic properties of the matrix.

For the highest molecular weight (M_w = 177.8 kDa)) phase separation of polymer-*g*-nanoparticles and homopolymer takes place. Here we observed a horizontal shift of the mastercurve toward higher frequencies and a vertical shift to lower moduli (Figure 6). The horizontal shift of G' and G'' to higher

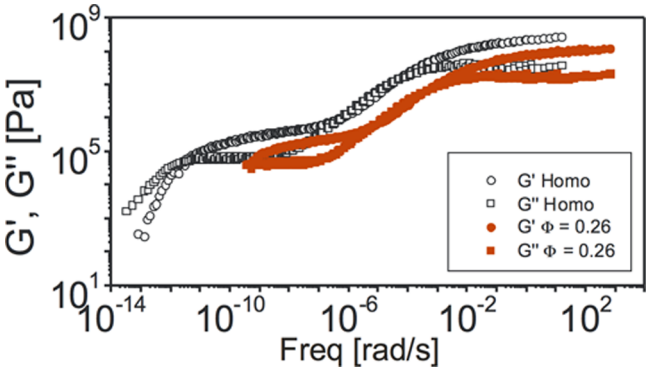

Figure 6. Mastercurves for blends of polymer-*g*-nanoparticles with homopolymers of M_w = 177.8 kDa for core volume fractions of 0.26 (filled symbols). The mastercurve of the neat homopolymer is represented by empty symbols.

frequencies due to addition of polymer-*g*-nanoparticles implies a reduction of the glass transition temperature. Indeed, T_g decreases form 75 °C for the homopolymer to 70 °C for ϕ_c = 0.26 and to 60 °C for ϕ_c = 0.49 (Figure 7).

We measured the plateau moduli for the sample with M_w = 177.8 kDa, which represents the vertical shift of the mastercurve. Due to addition of polymer-*g*-nanoparticles (ϕ_c = 0.26), the modulus reduces from 400 to 190 kPa. This reduction of −48% is attributed to the poor interaction of the polymer-*g*-nanoparticles with the surrounding high M_w matrix. The aggregates we have seen in SPM and GISAXS measurements in this case are hindering the matrix to entangle and thus causing defects in the melt leading to a decreased modulus. If the core volume fraction is increased to 0.49, the modulus of the polymer-*g*-nanoparticle clusters is contributing to the modulus of the composite, since almost half of the composite

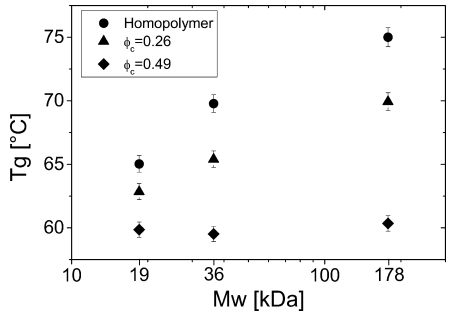

Figure 7. Glass transition temperatures $T_g(G''_{max})$ determined from temperature dependent G'' curves at a reference frequency of 1 rad/s for the neat homopolymer (dots), a particle volume fraction ϕ_c of 0.26 (triangles) and 0.49 (diamonds).

consists of polymer-*g*-nanoparticles. In this case the plateau modulus is measured to be 34 kPa.

From the plot of the glass transition temperature obtained from DMTA (Figure 7), we recognize two factors that reduce the T_g of the composite compared to the neat homopolymer. The first factor is the volume fraction (ϕ_c) of the polymer-*g*-nanoparticles. The highest reduction of T_g was observed for the composite with a particle volume fraction of 0.49 compared to the neat homopolymer. Given the fact that the filler loading is very high, this leads to a situation in which the T_g is effectively independent of matrix molecular weight. For the volume fraction (ϕ = 0.26) the internal interfacial area is smaller and the effect on T_g is less pronounced. In this case T_g decreased from 75 to 70 °C for the highest matrix M_w.

The second factor that influences the reduction of T_g is the molecular weight of the matrix. Obviously the reduction is relative to the T_g of the matrix polymer. The highest reduction of T_g from 75 to 60 °C (−19.5%) at ϕ_c = 0.49 was observed for the highest molecular weight (178 k). For lower molecular weight of the matrix the decrease in T_g was also lower, from 70 to 60 °C for the 36 kDa matrix and from 65 to 60 °C for the 19 kDa matrix.

To corroborate our structural model and to emphasize that the grafted polymer brushes are less compatible with high molecular weight matrices than with low M_w matrices, we conducted an in depth SPM analysis. When N/P is lower than one, the particles start to dewet from the surrounding matrix. To quantify this hypothesis, we calculated the contact angles of polymer-*g*-nanoparticles at homopolymer surfaces from SPM images. To do this, we analyze how much a particle peaks out of the surface and relate this to the particle radius R (cf., Figure 8).

The contact angle was then calculated by eq 2.

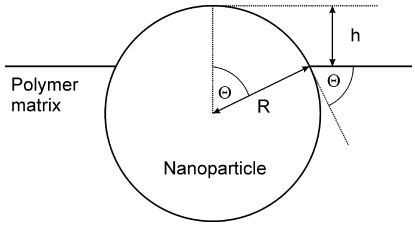

Figure 8. Determination of the contact angle Θ between a nanoparticle and a polymer matrix by measuring the height h of the particle peaking out of the matrix. The height values were obtained by SPM in our study.

DOI: 10.1021/am507572q
ACS Appl. Mater. Interfaces 2015, 7, 12380−12386

$$\cos\Theta = (R - h)/R \quad (2)$$

Here R is the radius of the particle and h the distance between the surface of the matrix and the top of a peaking out particle. A high contact angle indicates a weak interaction between the polymer matrix and the nanoparticle. A particle that "likes" the matrix should immerse into the matrix and show zero contact angle. This approach however has two limitations. First, it relies on the simultaneous presence of a particle and a matrix, therefore we are unable to probe the contact angle of the pure matrix and the pure particles alone. Second, since we can not include a series of reference materials with slowly changing energies, we are unable to determine surface energies from the contact angles. Nevertheless the SPM analysis enables us to map relative variations in contact energies in a self-contained way. For low molecular weight of the matrix (12k), we have deduced a low contact angle of 29° indicating good compatibility between polymer-*g*-nanoparticles and matrix polymer (Figure 9), this corresponds to a wet brush condition.

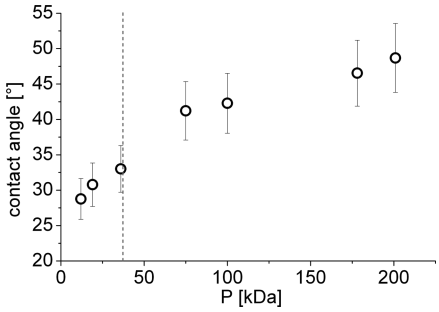

Figure 9. Contact angle of polymer-*g*-nanoparticles as a function of the molecular weight P of the matrix. The dashed line indicates $N/P = 1$.

As the matrix M_w is increased, also the contact angle increased. At the highest M_w of the matrix (201k) we deduced a contact angle of 49°, indicating that the increase in M_w forces the brush covered particles into the dry brush regime and consequently the particles dewet from the matrix. Again the miscibility of the brush covered particles depends on the N/P ratio. We find a change in slope above and below $N/P = 1$. This again shows that most structural properties are determined by the covering brush layer, irrespective of the cores softness.

CONCLUSIONS

From microscopy measurements we can conclude that homogeneous dispersion of the polymer-*g*-nanoparticles is only given for N/P ratios bigger than one (here P denotes the molecular weight of the homopolymer chain and N the molecular weight of brushes grafted on the nanoparticles). Moreover, the N/P ratio has direct consequences on the structure of the interfacial layer between grafted brushes and matrix. Contact angle measurements are a direct proof of the compatibility between a polymer-*g*-nanoparticle and a homopolymer matrix. Our results show that the polymer-*g*-nanoparticles form a nonwetting shell at high molecular weights of the matrix and in consequence, the concept of a liquid-like layer between the nonwetting shell and the matrix is supported by our experiments. As a result of this incompatibility a reduction of the T_g together with a reduction of the plateau modulus at high molecular weight of the matrix was observed. As the structural properties of the resulting composites are mainly determined by the N/P ratio, we conclude that the soft nanocomposites may be used as carrier systems in which the structural properties can be controlled independently from the loading state of the soft swellable cores.

ASSOCIATED CONTENT

Supporting Information

Details of the rheology experiments. This material is available free of charge via the Internet at http://pubs.acs.org.

AUTHOR INFORMATION

Corresponding Authors

*Tel: +49-6131-379-114. Fax: +49-6131-379-100. E-mail: berger@mpip-mainz.mpg.de.

*Tel: +49-201-183-2566. Fax: +49-201-183-100. E-mail: jochen.gutmann@uni-due.de.

Present Address

§J.S.G.: Department of Chemistry and Center for Nanointegration Duisburg-Essen (CENIDE), University of Duisburg-Essen, 45141 Essen, Germany.

Notes

The authors declare no competing financial interest.

ACKNOWLEDGMENTS

S.A.P. (BE 3286/1) and S.G.J.E. (GU 771/3) gratefully acknowledge financial support from the Deutsche Forschungsgemeinschaft (DFG) under the SPP1369 Priority Program (Polymer-Solid Contacts: Interfaces and Interphases). Furthermore, the help of Dr. K. Koynov and Andreas Hanewald during the rheology measurements, the support of Dr. S. V. Roth during GISAXS measurements, and the provision of beamtime by the HASYLAB is gratefully acknowledged.

REFERENCES

(1) Winey, K. I.; Vaia, R. A. Polymer Nanocomposites. *MRS Bull.* **2007**, *32*, 314−319.

(2) Ajayan, P. M.; Schadler, L. S.; Braun, P. V. *Nanocomposite Science and Technology*; Wiley-VCH: Weinheim, 2003.

(3) Wang, X. R.; Foltz, V. J.; Rackaitis, M.; Böhm, G. G. A. Dispersing Hairy Nanoparticles in Polymer Melts. *Polymer* **2008**, *49*, 5683−5691.

(4) Corbierre, M. K.; Cameron, N. S.; Sutton, M.; Laaziri, K.; Lennox, R. B. Gold Nanoparticle/Polymer Nanocomposites: Dispersion of Nanoparticles as a Function of Capping Agent Molecular Weight and Grafting Density. *Langmuir* **2005**, *21*, 6063−6072.

(5) Xu, C.; Ohno, K.; Ladmiral, V.; Composto, R. J. Dispersion of Polymer-Grafted Magnetic Nanoparticles in Homopolymers and Block Copolymers. *Polymer* **2008**, *49*, 3568−3577.

(6) Lan, Q.; Francis, L. F.; Bates, F. S. Silica Nanoparticle Dispersions in Homopolymer versus Block copolymer. *J. Polym. Sci., Part B: Polym. Phys.* **2007**, *45*, 2284−2299.

(7) Green, D. L.; Mewis, J. Connecting the Wetting and Rheological Behaviors of Poly(Dimethylsiloxane)-Grafted Silica Spheres in Poly(Dimethylsiloxane) Melts. *Langmuir* **2006**, *22*, 9546−9553.

(8) Dutta, N.; Green, D. Nanoparticle Stability in Semidilute and Concentrated Polymer Solutions. *Langmuir* **2008**, *24*, 5260−5269.

(9) Ohno, K.; Morinaga, T.; Takeno, S.; Tsujii, Y.; Fukuda, T. Suspensions of Silica Particles Grafted with Concentrated Polymer Brush: Effects of Graft Chain Length on Brush Layer Thickness and Colloidal Crystallization. *Macromolecules* **2007**, *40*, 9143−9150.

(10) Akcora, P.; Kumar, S. K.; Moll, J.; Lewis, S.; Schadler, L. S.; Li, Y.; Benicewicz, B. C.; Sandy, A.; Narayanan, S.; Illavsky, J.; Thiyagarajan, P.; Colby, R. H.; Douglas, J. F. "Gel-like" Mechanical Reinforcement in Polymer Nanocomposite Melts. *Macromolecules* **2010**, *43*, 1003−1010.

DOI: 10.1021/am507572q
ACS Appl. Mater. Interfaces 2015, 7, 12380−12386

(11) Bansal, A.; Yang, H. C.; Li, C. Z.; Benicewicz, R. C.; Kumar, S. K.; Schadler, L. S. Controlling the Thermomechanical Properties of Polymer Nanocomposites by Tailoring the Polymer−Particle Interface. *J. Polym. Sci., Part B: Polym. Phys.* **2006**, *44*, 2944−2950.
(12) Hamming, L. M.; Qiao, R.; Messersmith, P. B.; Brinson, L. C. Effects of Dispersion and Interfacial Modification on the Macroscale Properties of TiO(2) Polymer-Matrix Nanocomposites. *Compos. Sci. Technol.* **2009**, *69*, 1880−1886.
(13) Zhang, Q.; Archer, L. A. Interfacial Friction and Adhesion of Cross-Linked Polymer Thin Films Swollen with Linear Chains. *Langmuir* **2002**, *18*, 10435−10442.
(14) Tangchantra, N.; Kruenate, J.; Aumnate, C.; Sooksomsong, T. The Effect of Surface Modification of TiO(2) on Mechanical Properties of Polyethylene Composite Film. *Funct. Sens. Mater.* **2010**, *93*−*94*, 300−303.
(15) Navarro, M.; Aparicio, C.; Charles-Harris, M.; Ginebra, M. P.; Engel, E.; Planell, J. A. In *Ordered Polymeric Nanostructures at Surfaces*, Advances in Polymer Science 200; Springer-Verlag: Berlin, 2006; pp 209−231.
(16) Akcora, P.; Kumar, S. K.; Sakai, V. G.; Li, Y.; Benicewicz, B. C.; Schadler, L. S. Segmental Dynamics in PMMA-Grafted Nanoparticle Composites. *Macromolecules* **2010**, *43*, 8275−8281.
(17) Pihan, S. A.; Emmerling, S. G. J.; Butt, H.-J.; Gutmann, J. S.; Berger, R. Nanowear in a Nanocomposite Reinforced Polymer. *Wear* **2011**, *271*, 2852−2856.
(18) Gohr, K.; Pakula, T.; Tsutsumi, K.; Schärtl, W. Dynamics of Copolymer Micelles in an Entangled Homopolymer Matrix. *Macromolecules* **1999**, *32*, 7156−7165.
(19) Schärtl, W.; Tsutsumi, K.; Kimishima, K.; Hashimoto, T. FRS Study of Diffusional Processes in Block Copolymer/Homopolymer Blends Containing Glassy Spherical Micelles. *Macromolecules* **1996**, *29*, 5297−5305.
(20) Sun, Z. C.; Gutmann, J. S. Synthesis of TiO_2 Nanoparticles in Ultrathin Block Copolymer Films—An Integral Geometry Study. *Phys. A* **2004**, *339*, 80−85.
(21) Schexnailder, P.; Schmidt, G. Nanocomposite Polymer Hydrogels. *Colloid Polym. Sci.* **2009**, *287*, 1−11.
(22) Oh, J. K.; Drumright, R.; Siegwart, D. J.; Matyjaszewski, K. The Development of Microgels/Nanogels for Drug Delivery Applications. *Prog. Polym. Sci.* **2008**, *33*, 448−477.
(23) Okano, T.; Bae, Y. H.; Jacobs, H.; Kim, S. W. Thermally On Off Switching Polymers for Drug Permeation and Release. *J. Controlled Release* **1990**, *11*, 255−265.
(24) Feil, H.; Bae, Y. H.; Feijen, J.; Kim, S. W. Mutial Influence of pH and Temperature on the Swelling of Ionizable and Thermosensitive Hydrogels. *Macromolecules* **1992**, *25*, 5528−5530.
(25) Hirasa, O. Research Trends of Stimuli-Responsive Polymer Hydrogels. *Jpn. J. Intell. Mater. Syst. Struct.* **1993**, *4*, 538−542.
(26) Ahearne, M.; Yang, Y.; El Haj, A. J.; Then, K. Y.; Liu, K.-K. Characterizing the Viscoelastic Properties of Thin Hydrogel-Based Constructs for Tissue Engineering Applications. *J. R. Soc., Interface* **2005**, *2*, 455−463.
(27) Muniz, E. C.; Geuskens, G. Compressive Elastic Modulus of Polyacrylamide Hydrogels and Semi-IPNs with Poly(*N*-Isopropylacrylamide). *Macromolecules* **2001**, *34*, 4480−4484.
(28) Iza, M.; Stoianovici, G.; Viora, L.; Grossiord, J. L.; Couarraze, G. Hydrogels of Poly(Ethylene Glycol): Mechanical Characterization and Release of a Model Drug. *J. Controlled Release* **1998**, *52*, 41−51.
(29) Kim, J.; Green, P. F. Phase Behavior of Thin Film Brush-Coated Nanoparticles/Homopolymer Mixtures. *Macromolecules* **2010**, *43*, 1524−1529.
(30) Meli, L.; Arceo, A.; Green, P. F. Control of the Entropic Interactions and Phase Behavior of Athermal Nanoparticle/Homopolymer Thin Film Mixtures. *Soft Matter* **2009**, *5*, 533−537.
(31) Jakuczek, L.; Gutmann, J. S.; Müller, B.; Rosenauer, C.; Zuchowska, D. Well-Defined Core-Shell Structures Based on Silsesquioxane Microgels: Grafting of Polystyrene via ATRP and Product Characterization. *Polymer* **2008**, *49*, 843−856.
(32) Baumann, F.; Schmidt, M.; Deubzer, B.; Geck, M.; Dauth, J. On the Preparation of Organosilicon μ-Spheres—A Polycondensation in μ-Emulsion. *Macromolecules* **1994**, *27*, 6102−6105.
(33) Emmerling, S. G. J. Polymer Brushes: Wetting Properties and Micro-Patterning. Ph.D. Thesis, Johannes Gutenberg University, Mainz, Germany, 2010.
(34) Ramakrishnan, A.; Dhamodharan, R. Facile Synthesis of ABC and CBABC Multiblock Copolymers of Styrene, Tert-Butyl Acrylate, and Methyl Methacrylate via Room Temperature ATRP of MMA. *Macromolecules* **2003**, *36*, 1039−1046.
(35) Roth, S. V.; Dohrmann, R.; Dommach, M.; Kuhlmann, M.; Kroger, I.; Gehrke, R.; Walter, H.; Schroer, C.; Lengeler, B.; Müller-Buschbaum, P. Small-Angle Options of the Upgraded Ultrasmall-Angle X-ray Scattering Beamline BW4 at HASYLAB *Rev. Sci. Instrum.* **2006**, *77*.
(36) Wolkenhauer, M.; Bumbu, G. G.; Cheng, Y.; Roth, S. V.; Gutmann, J. S. Investigation of Micromechanical Cantilever Sensors with Microfocus Grazing Incidence Small-Angle X-ray Scattering. *Appl. Phys. Lett.* **2006**, *89*, No. 054101.
(37) Yoneda, Y. Anomalous Surface Reflection of X-rays. *Phys. Rev.* **1963**, *131*, 2010.
(38) Ehrenstein, G. W.; Riedel, G.; Trawiel, P. *Praxis der Thermischen Analyse von Kunststoffen*, 2nd ed.; Hanser Fachbuch: München, Germany, 2003.
(39) Liu, J.; Cao, D.; Zhang, L. Molecular Dynamics Study on Nanoparticle Diffusion in Polymer Melts: A Test of the Stokes−Einstein Law. *J. Phys. Chem. C* **2008**, *112*, 6653−6661.
(40) Forrest, J. A.; Mattsson, J. Reductions of the Glass Transition Temperature in Thin Polymer Films: Probing the Length Scale of Cooperative Dynamics. *Phys. Rev. E* **2000**, *61*, R53−R56.
(41) Sharp, J. S.; Teichroeb, J. H.; Forrest, J. A. The Properties of Free Polymer Surfaces and Their Influence on the Glass Transition Temperature of Thin Polystyrene Films. *Eur. Phys. J. E: Soft Matter Biol. Phys.* **2004**, *15*, 473−487.
(42) Zhou, T. H.; Ruan, W. H.; Yang, J. L.; Rong, M. Z.; Zhang, M. Q.; Zhang, Z. A Novel Route for Improving Creep Resistance of Polymers using Nanoparticles. *Compos. Sci. Technol.* **2007**, *67*, 2297−2302.
(43) Meth, J. S.; Zane, S. G.; Chi, C.; Londono, J. D.; Wood, B. A.; Cotts, P.; Keating, M.; Guise, W.; Weigand, S. Development of Filler Structure in Colloidal Silica−Polymer Nanocomposites. *Macromolecules* **2011**, *44*, 8301−8313.
(44) Wind, M.; Graf, R.; Renker, S.; Spiess, H. W.; Steffen, W. Structure of Amorphous Poly-(Ethylmethacrylate): A Wide-Angle X-ray Scattering Study. *J. Chem. Phys.* **2005**, *122*, No. 014906.

DOI: 10.1021/am507572q
ACS Appl. Mater. Interfaces 2015, 7, 12380−12386